



## In situ X-ray diffraction studies of iron to Earth-core conditions

Yanzhang Ma<sup>a,\*</sup>, Maddury Somayazulu<sup>b</sup>, Guoyin Shen<sup>c</sup>, Ho-kwang Mao<sup>b</sup>,  
Jinfu Shu<sup>b</sup>, Russell J. Hemley<sup>b</sup>

<sup>a</sup> Department of Mechanical Engineering, Texas Tech University, Box 41021, Lubbock, TX 79409, USA

<sup>b</sup> Geophysical Laboratory, Carnegie Institution of Washington, 5251 Broad Branch Rd. NW, Washington, DC 20015, USA

<sup>c</sup> Consortium for Advanced Radiation Sources, University of Chicago, Chicago, IL 60637, USA

Received 30 January 2003; received in revised form 29 May 2003; accepted 24 June 2003

### Abstract

The high-pressure, high-temperature behavior of iron has been investigated to 161 GPa and 3000 K by in situ synchrotron X-ray diffraction with double-side laser-heated diamond anvil cells. We found that only  $\alpha$ -,  $\gamma$ - and  $\epsilon$ -Fe can be clearly verified as the stable solid phase in the  $P$ – $T$  range studied. Only  $\epsilon$ -Fe is observed from deep lower mantle ( $\sim 1500$  km) to outer core conditions. Within the  $P$ – $T$  range examined, we did not observe a significant change with pressure or temperature on the  $c/a$  ratio of  $\epsilon$ -Fe. The melting curve of iron has been determined to 105 GPa. A Lindeman law fit gives a melting point of iron at the inner core boundary of 5800 ( $\pm 200$ ) K, which provides an upper bound on the temperature at that depth. We also examine numerous experimental factors that may complicate the analysis of high  $P$ – $T$  diffraction data, and discuss the effects of sample stress on the X-ray diffraction results.

© 2004 Elsevier B.V. All rights reserved.

**Keywords:** Iron; Phase diagram; High pressure; High temperature; X-ray diffraction

### 1. Introduction

The Earth's core is mainly composed of iron and an additional light element component. Thus the structural properties and phase diagram of iron at core conditions are critical for understanding this most inaccessible region of our planet. From seismology, the inner core is known to be solid whereas the outer core is liquid. At the inner core boundary ICB, this iron-rich material crystallizes and releases latent heat and gravitational energy that at least in part drives the dynamo (Anderson, 1990). The melting temperature of iron at ultrahigh (i.e., megabar) pressures thus gives

a bound on the temperature regime of the core. In addition, there is evidence for unusual elastic anisotropy of the inner core (e.g., Song and Helmberger, 1993), a property that is controlled by the crystal structure of the material. Hence, investigation of the high-pressure melting curve, phase relations, and lattice parameters of the stable phases of iron at deep Earth conditions is of fundamental geophysical importance.

Iron has been reported to have at least six phases based on X-ray diffraction at high pressure and temperature, i.e.,  $\alpha$ , body-centered-cubic (b.c.c.);  $\gamma$ , face-centered-cubic (f.c.c.);  $\delta$ , b.c.c.;  $\epsilon$ , hexagonal closed-packed (h.c.p.); double-h.c.p. phase (d.h.c.p.); and an orthorhombic phase. The  $\alpha$ -,  $\gamma$ -, and  $\delta$ -phases at lower pressures are well established and broadly accepted. The  $\epsilon$ -phase, first observed at a high pressure and room temperature (Takahashi and Bassett,

\* Corresponding author. Tel.: +1-806-742-0971;

fax: +1-806-742-3540.

E-mail address: [y.ma@coe.ttu.edu](mailto:y.ma@coe.ttu.edu) (Y. Ma).

1964), has been proved a dominant phase in a wide  $P$ – $T$  range approaching Earth's core conditions. Other high-pressure phases of iron have been observed at temperatures near its high-pressure melting line. A phase (called  $\beta$ ) was proposed based on reported temperature–laser power relations and high  $P$ – $T$  X-ray diffraction (Saxena et al., 1995; Dubrovinsky et al., 1998, 2000). Other experiments revealed a double-hexagonal close-packed structure (d.h.c.p. or  $\epsilon'$ ) that was believed to be identical to the  $\beta$ -phase and identified as metastable (Yoo et al., 1995). An orthorhombic phase was also reported at 30–100 GPa and temperatures to 2370 K (Andrault et al., 1997). These results, however, could not be reproduced in other experiments (e.g., Shen et al., 1998), where it was found that the  $\epsilon$ -h.c.p. phase persists to the melting points of iron over a range of pressures. This is consistent with the proposal that the identified phases were either metastable (Yoo et al., 1995) or incorrectly identified (Yoo et al., 1997; see also Hemley and Mao, 2001a). In view of the continuing discussion of these issues and the importance for understanding the core (e.g., Boehler, 2000), further clarification of the high-pressure solid phases of iron and their stability fields, as well as discussion of the relevant experimental details, is needed.

The high-pressure melting curve of iron is also controversial (see Hemley and Mao, 2001a). Although it has been extensively investigated by many available experimental methods, including Joule heating (Mao et al., 1987; Boehler, 1986), laser heating with visual observation (Williams et al., 1987; Boehler, 1993), laser heating with synchrotron X-ray diffraction (Shen et al., 1998), and shock compression (Brown and McQueen, 1986; Yoo et al., 1993), most of the results are inconsistent with each other, particularly at higher pressures where direct measurements become difficult. The differences in melting temperatures among different determinations can exceed 1000 K when pressures approach the megabar range. Thus, as in the case of the solid-phase studies, it is necessary to carefully re-examine earlier results and further investigate the solid–liquid equilibrium line to pressures of the Earth's core.

The continued development of synchrotron radiation and diamond cell laser heating techniques has resulted in an ideal method for the study of materials under the extreme  $P$ – $T$  conditions of the Earth's core

(Mao et al., 1997; Shen and Heinz, 1998; Hemley et al., 2002). However, differences in techniques, distinctions that are often subtle, can have major effects on the experimental results. With the increasing numbers of experimental studies, however, the evaluation of experimental factors becomes particularly important. For example, we find that some earlier disputes on the behavior of iron at high pressures and temperatures can be attributed to the experimental accuracy of specific methods and the degree to which key experimental factors can be manipulated and controlled. This attention to experimental detail is crucial for testing the broad range of increasingly accurate theoretical predictions of the behavior of iron (and iron alloys) at Earth's core conditions (e.g., Alfè et al., 1999, 2000; Steinle-Neumann et al., 2001).

In this paper, we present the results of experimental studies of the high  $P$ – $T$  phase diagram and structural properties of iron to 161 GPa and 3000 K obtained using recent improvements in diamond cell laser heating/synchrotron X-ray diffraction techniques. Preliminary reports of some of this data have been mentioned in earlier review articles (Shen and Heinz, 1998; Hemley and Mao, 2001a). Here we present additional experimental details that are critically important for assessing the accuracy of the results, as well as new data and analyses of the high  $P$ – $T$  behavior of iron to compare with recent theoretical predictions.

## 2. Experimental

### 2.1. Sample loading

We employed symmetric diamond anvil cells with flat diamonds for lower pressures experiments and beveled diamonds at higher pressures (over 60 GPa). Flat diamond culet sizes ranged from 300 to 400  $\mu\text{m}$ , and the beveled diamond culets from 80 to 110  $\mu\text{m}$ . Rhenium and stainless steel gaskets were used in these experiments; gaskets were pre-indented to 20  $\mu\text{m}$  or less before drilling holes for the sample chambers. The diameter of the sample chambers were larger than 120  $\mu\text{m}$  with flat diamonds, and were the same sizes as the diamond culet for beveled diamonds. NaCl, MgO, and Al<sub>2</sub>O<sub>3</sub> served as pressure media and heating insulators in our experiments; these materials were pressed

to form transparent flakes, and sandwiched the sample on either side within the sample chamber. Experiments were carried out with all three pressure media to verify their possible chemical reactions with the sample. The sample was pure iron powder with grain sizes smaller than  $1\ \mu\text{m}$ , compressed into a  $\sim 5\ \mu\text{m}$  thick and  $30\text{--}40\ \mu\text{m}$  wide flake before loading. During sample loading, the iron was located at the center, and care was taken to avoid bridging the gasket by the sample, i.e., no portion of the sample was in contact with the edges of the gasket during the course of the experiment. We also removed all sample debris on the gasket within the diamond flat surface before compression. In the runs with beveled diamonds, we loaded the samples such that no gasket remained on top of the diamond culet after increasing the pressure (Fig. 1). After loading the sample, we evacuated and filled the cell with argon repeatedly over a period of several hours, and then kept it in an oven at a temperature of  $90\ ^\circ\text{C}$  in an environment of flowing Ar gas for 72 h to eliminate water and oxygen. In our experiments below 60 GPa, we also used Ar gas as a pressure medium, and  $5\ \mu\text{m}$ -sized ruby chips as spacers to keep the sample from contacting the diamond before filling with liquid argon. Other aspects of these runs are similar to those described above. The iron equation of state was used as a pressure scale (Mao et al., 1990).

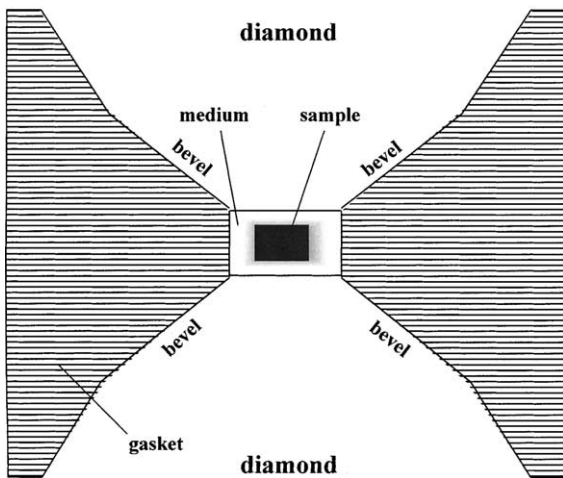


Fig. 1. Cross-section of a sample loaded in a diamond anvil cell with beveled diamonds. Note that the size of the gasket hole is the same as that of the diamond culet.

## 2.2. Laser heating

We conducted our experiments both at GSECARS, Sector 13 of the Advanced Photon Source (APS), Argonne National Laboratory, and beamline X17B of the National Synchrotron Light Source (NSLS), Brookhaven National Laboratory. In the experiments, we used a double-sided laser heating system with a dual imaging setup, which allows us to visually observe the sample during the heating process (Fig. 2). We measured the temperature by the thermal radiation method in these systems. In the system at APS, two Nd:YLF single-mode lasers are combined together, with a total output of 105 W, which has been proven sufficient to generate stable temperatures higher than 3000 K. One laser was operated in TEM<sub>00</sub> mode and the other in the donut mode to create a homogeneous flat top power distribution (with radial gradient less than 3%) at the laser spot center. A detailed description of this system and an explanation of the experimental method has been published previously (Shen et al., 2001). At NSLS we used a multimode YAG laser with output power in the order of 50 W.

## 2.3. Synchrotron X-ray diffraction

We carried out our in situ high  $P$ – $T$  X-ray diffraction measurements of iron using energy-dispersive synchrotron radiation methods. The experiments above 60 GPa were carried out at the APS. With the insertion of the linear arrays of north–south permanent magnets with alternating polarity in a straight section, the APS provides a brilliant beam with very low divergence ( $283 \times 40\ \mu\text{rad}$ ). This has yielded significant improvements in the quality of in situ high  $P$ – $T$  diffraction measurements at megabar pressures and thousands of degrees Kelvin with diamond cells, where the sample is thin and the gasket hole becomes much smaller than originally drilled. The low divergence of the X-ray beam helps to eliminate the detectable scattering from the gasket and other contamination on it. We reduced the size of the X-ray beam using two perpendicular slits with paired tungsten carbide cubes having sharp edges, and eliminated the tails of the beam with another pairs of slits made out of tungsten plates. With this configuration, we obtained X-ray beam sizes of less than  $8\ \mu\text{m} \times 10\ \mu\text{m}$  at the sample position. No X-ray focusing mirrors were used in experiments at

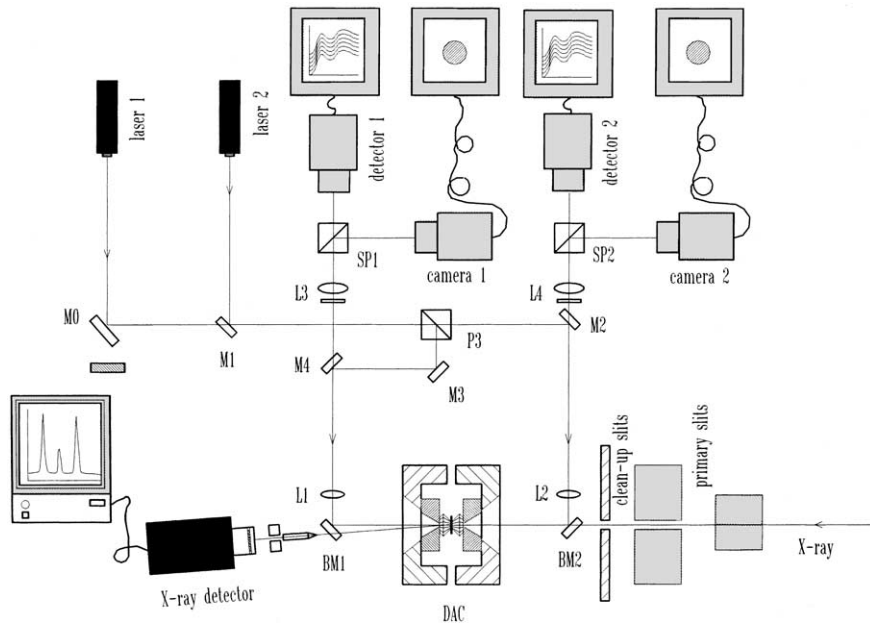


Fig. 2. Schematic diagram of synchrotron X-ray diffraction system with double-sided laser heating apparatus.

APS. Several experiments below 60 GPa were carried out at NSLS to verify the phase boundaries. In these runs, we used a Kirkpatrick-Baez mirror to enhance the beam intensity; the X-ray beam size at the sample position was  $25 \mu\text{m} \times 30 \mu\text{m}$ .

With energy-dispersive synchrotron X-ray diffraction, a well-resolved diffraction pattern of a strongly scattering sample such as iron can be collected within several seconds. This allows real-time capture of the signal that can reveal ongoing processes taking place in the sample at a given pressure and temperature. As conventionally applied, however, it does not permit any signal to be collected away from the point of detection; hence, information away from the detecting point is not available. This effect becomes more critical at high temperatures where recrystallization and crystal coarsening from an originally fine-grained powder sample can occur. To overcome such an effect in phase identification experiments, we developed a two-dimensional X-ray diffraction method for double-sided laser heating of diamond anvil cells (Ma et al., 2001), where the diamond cell is mounted on a high-precision rotation stage and the sample center coincides with its rotation center. We estimated the off-center error caused by the alignment to be less

than  $2\text{--}3 \mu\text{m}$ . Thus, it is impossible for the sample center position to drift out of the flat part of the heating spot, which is about  $25 \mu\text{m}$  in diameter and fully covers the X-ray beam.

We used the rotating diamond cell method (both continuous and step-wise rotation) in our experiments. In the continuous-rotation method, we kept the sample rotating at a preset speed during data collection; the diffracted signals detected within all covered angles are added to make one pattern producing a good average spectrum. In the step-wise-rotation method, we rotated the sample by discrete steps and collected the signal at each rotation angle. This method is more effective for simultaneously detecting the existence of new peaks without accumulating the high background characteristic of the continuous-rotation method. The possible failure to detect any signal between two steps can also be avoided by decreasing the step size to correspond to the system's spatial resolution in the rotation angle, which is defined by the tip opening and collimation system of the detector. The step-rotation method was used to identify the high-pressure phase of iron to 161 GPa. We selected several rotation steps to detect possible peaks at angles as low as  $0.5^\circ$ . We could not resolve any change in the diffraction

pattern at steps below  $5^\circ$ . At steps higher than  $5^\circ$ , we observed intensity changes between steps. Therefore, we chose  $5^\circ$  steps in most of our experiments.

The application of the cell-rotation methods is facilitated by high-resolution CCD cameras in the laser heating system, where we use the X-ray-induced visible fluorescence from the pressure medium in the cell to locate the X-ray position, then move the sample on the rotation center to this position and couple the lasers from both sides to it. Such an alignment allows the X-ray beam and the lasers from two sides of the sample to be coincident within  $\sim 2\text{--}3\ \mu\text{m}$ . Another possible effect of the cell rotation is that the laser coupling position may drift during heating because of the differences in diamond thickness in different directions (i.e., within a machining error). This effect was proved minor in our experiments, and can be further eliminated by aligning the laser beam perpendicular to the diamond surfaces.

### 3. Results and Discussion

#### 3.1. Artifacts and experimental errors

High-pressure/high-temperature phase identification using synchrotron X-ray and laser-heated diamond anvil cell techniques cell involves many advanced experimental methods, and error analysis becomes a most important issue. Disputes about on the high  $P$ – $T$  phases of iron are commonly related to the estimation of certain experimental errors, which are hard to clarify. We feel it is highly valuable and beneficial to evaluate some common errors involved in the experiments that have long been ignored.

Fig. 3 shows X-ray diffraction patterns acquired in some of the experiments carried out to deliberately introduce systematic errors. Most of the diffraction peaks appear to show a broad shoulder. These patterns are unstable during heating, and the shoulders can diminish after some fine alignment. Such a phenomenon indicates that the shoulders, sometimes considered as diffraction peaks, are directly related to the effects of heating under pressure. The pressure gradient caused by stress in the sample chamber of a diamond anvil cell during compression has been studied since the earliest application of the device (e.g., Sung et al., 1977). A typical radial pressure gradient for NaCl, a soft pres-

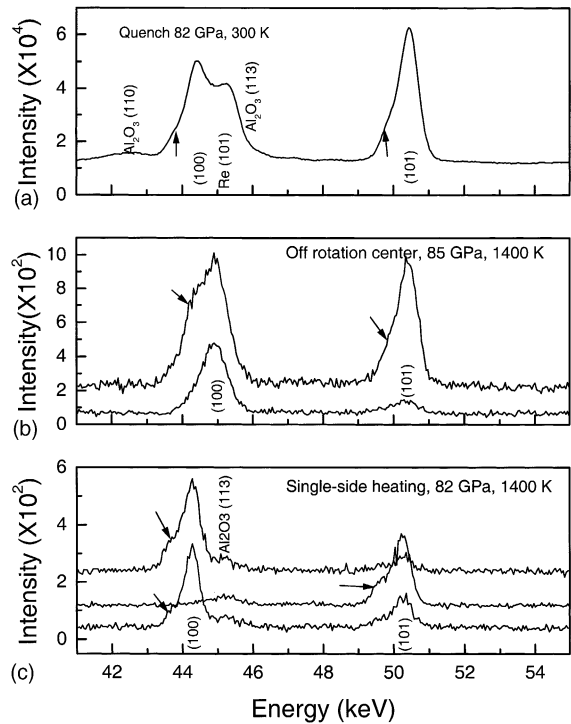


Fig. 3. Examination of errors associated with X-ray diffraction patterns of iron. (a) Temperature-quenched sample heated to 1400 K at 82 GPa through  $360^\circ$  rotation; (b) in situ pattern at 85 GPa and 1400 K at different rotation angles with heating spot away from the diffracting position; (c) in situ pattern at 82 GPa and 1400 K with one-sided heating. Arrows point to the shoulders in the patterns.

sure medium often used in laser heating, has been measured to be  $\sim 5\ \text{GPa}/50\ \mu\text{m}$  at 35–40 GPa (Meade and Jeanloz, 1988), whereas iron itself and other pressure media can give much larger gradients. Recent experimental results show that the stress difference between the axial and radial directions can cause as high as a 20% difference in the  $d$ -spacings of iron at 50 GPa (Mao et al., 1998). Even argon, the conventional pressure medium, has a 10% radial–axial pressure difference at 60 GPa (Mao et al., in preparation; Hemley and Mao, 2001b). At ambient temperature, the effect of such a stress can only broaden the diffraction peaks, while at high temperature, the effects of stress can be much more complicated.

Another experimental issue of concern with laser-heated diamond cell techniques is the temperature gradient across the sample, which can be affected by several factors, including the difference in power

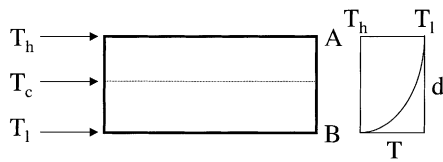


Fig. 4. Schematic diagram of the temperature-distribution effect on  $d$ -spacings. Left: temperature distribution of a heated spot along the axial direction illustrating the temperature difference between the two sides:  $T_h$ , highest temperature (A side);  $T_l$ , lowest temperature (B side);  $T_c$ , stress relaxation critical point. Right:  $d$ -spacing changes with temperature.

input from the two sides, quality of sample loading and processing, and alignment of the laser heating system. The early one-sided heating experiment typically produced large axial temperature gradient as a result of the power drop-off from one side of the cell to the other. Even with the improved double-sided laser heating technique, this phenomenon may still exist. From our visual observations, we can clearly observe the glowing heated spot (above 1200 K) from one side, while the other side with an equal power input remains dark (below 1000 K). The measured temperature difference between the two sides can be as high as 1000 K.

Experimental results also show that even though the stress is released inside the heating spot at temperatures higher than 1200 K (unpublished data), pressure gradients still exist outside and on the border of the heating spot (see also Shim et al., 2000). With the potential buildup of stress and the manner in which stress can be released with increasing temperature, we recognize that the assumed experimental condition may also cause the diffraction peaks to split. In our model we assume a laser-heated sample as shown in Fig. 4, with side A at higher temperature,  $T_h$ , and side B at lower temperature,  $T_l$ . The temperature distribution between A and B continuously decreases from  $T_h$  to  $T_l$ . Our experimental data suggests the existence of a  $T_c$ , the temperature at a critical point of stress relaxation at high pressure. When  $T_l < T_c < T_h$ , a two-layer sample is created: one layer with temperatures higher than  $T_c$  and another with a temperature lower than  $T_c$ . In the high-temperature layer, the stress is released, while in the low-temperature layer the stress still exists. Because of this stress release, the  $d$ -spacings accordingly adopt the same value in every direction, and the diffracted peak could be shifted by as much as

20%. This effect has also been extensively discussed by Kavner and Duffy (2001). The X-ray beam passes through both layers, and the detector collects the scattered signal from both the stressed and unstressed layers. Hence we can almost certainly expect a splitting of the diffraction peaks. We demonstrated this effect by heating an iron sample from one side to 1400 K (thermal emission was recorded from one side whereas the other side remained dark). We clearly observed splitting of the peaks (i.e., shoulders appeared on the iron (1 0 0) and (1 0 1) peaks), similar to patterns reported in single-sided laser heating experiments (Fig. 3c).

Moreover, even for a well-controlled axial temperature distribution (i.e., well-aligned double-sided laser heating), the radial temperature distribution may also complicate the measurements. An ideal radial temperature distribution has a flattened peak with a sharply decreasing half-Gaussian-shaped edge (Mao et al., 1997). The flat top can range from as small as several microns to several tens of microns. The temperature distribution within this spot is far from homogeneous, in the case of an X-ray measurement, the probe beam is comparable with, or even bigger than, the heating spot. We must also take into account other experimental factors, such as the mismatch of the laser heating and X-ray diffracted spots, and cell translation during and after heating, because of the typical symmetric thermal expansion of the cell and its holder. To test these effects, we intentionally mismatched the X-ray beam with the laser heating spot by 10–20  $\mu\text{m}$  at high pressures; all the clearly resolved peaks produce a shoulder when the collecting time was long enough (i.e., producing diffraction patterns similar to those depicted in Fig. 3b and c). This phenomenon disappeared when the laser heating spot, X-ray beam, and sample were well aligned.

Another important factor that can adversely affect the experimental result is X-ray diffraction from the gasket. As can be inferred from Fig. 5, we can see that the source X-ray distribution also has a Gaussian-shaped space intensity distribution. Also, we need to further consider the method used to generate a highly collimated X-ray beam. For example, scattering from the slits used to define the X-ray beam size and the “wings” (extra intensity away from the beam center) generated from focusing mirrors can affect the diffraction pattern. The signals diffracted by these unexpected sources are usually negligible.

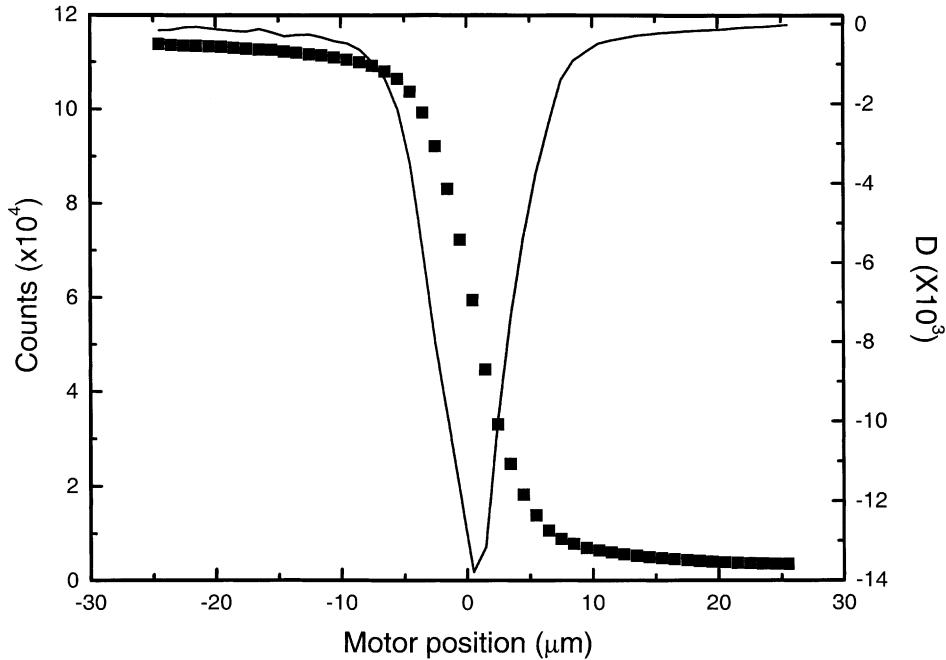


Fig. 5. Spatial distribution of the X-ray beam as shown by the sharp edge in a step scan. Left axis (solid square marks): detected counts with scan motor position; right axis (solid curve): differential of the intensity (counts) with motor position.

However, under the special circumstances associated with laser-heated diamond anvil cell experiments, these effects must be carefully considered. In most cases, the sample thickness is about one-third that of the gasket. We can reasonably expect that 10% of the peak X-ray intensity can easily generate detectable diffraction from the gasket. When a strong scatterer such as rhenium is adopted as a gasket material, the X-ray intensity required to generate a signal from the gasket can be low. The scatter due to the wings of the X-ray beam previously mentioned can also be intense; their effect on the diffraction data should be carefully checked.

We have tested these effects in our experiments. We used a synchrotron X-ray source with a beam size of  $8\ \mu\text{m} \times 10\ \mu\text{m}$  obtained with two pairs of slits. The rhenium gasket hole was  $80\ \mu\text{m}$  in diameter, and a  $30\ \mu\text{m}$ -sized iron sample was loaded in the center of the sample chamber. When the X-ray and laser were well aligned at the center of the sample, we clearly obtain diffraction patterns that are characteristic of the pure h.c.p. phase of iron at high pressures and high temperatures. If the X-ray beam shifts

by  $10\ \mu\text{m}$  (the magnitude of this shift can be easily caused by the thermal expansion of parts of the cell or its mounts), the diffraction from the gasket appears as shoulders on the iron peaks (Fig. 3a). Some of these shoulders have intensities comparable to those of the iron peaks. These rhenium peaks disappear after the sample is re-centered with the X-ray beam. This phenomenon is reproducible; we conclude that the area affected by scattering from the gasket can be  $20\text{--}30\ \mu\text{m}$  larger in each direction than the beam size. This result strongly suggests that experiments with gasket hole diameters less than the sum of the X-ray beam size plus  $2 \times 30\ \mu\text{m}$  should be carefully checked for any scattering from the gasket. Further, the mechanical mounting of the diamond cell can shift by  $\sim 10\ \mu\text{m}$  on heating. Frequent checking of the position of the sample relative to X-ray and laser beams (e.g., by X-ray transmission scans) is therefore required to ensure accurate high  $P$ – $T$  measurements. We conclude that a narrow, well-defined X-ray beam and a homogeneous temperature distribution are critical for high  $P$ – $T$  phase X-ray diffraction for obtaining quality data.

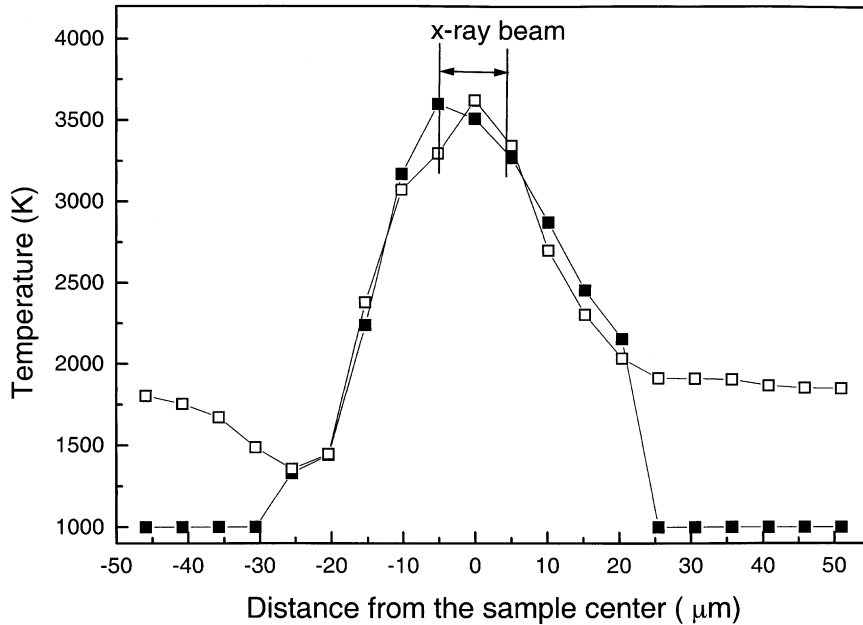


Fig. 6. Temperature distribution compared with the X-ray beam size for the laser heating at 105 GPa and 3500 K on the sample.

### 3.2. $P$ - $T$ stability of $\epsilon$ -Fe

As discussed by Shen et al. (2001), the laser heating method adopted at GSECARS has a highly improved temperature distribution relative to previous systems. The temperature difference within the dimension of the X-ray beam and between the two sides of the sample can be as low as 30 K. Fig. 6 shows a temperature distribution at 105 GPa and 3500 K. The temperature

gradient within the X-ray range is about  $\pm 100$  K at this pressure, which can be considered as the maximum error in our experiments. An X-ray diffraction image of iron at 161 GPa and 2410 K at rotation angles from 0 to  $90^\circ$  at  $5^\circ$  steps with data collected for 30 s at each step is presented in Fig. 7. The dark regions represent corresponding photon counts at certain energies and rotation angles. The dark lines (mostly diffraction lines) are straight and smooth, indicating homogenous

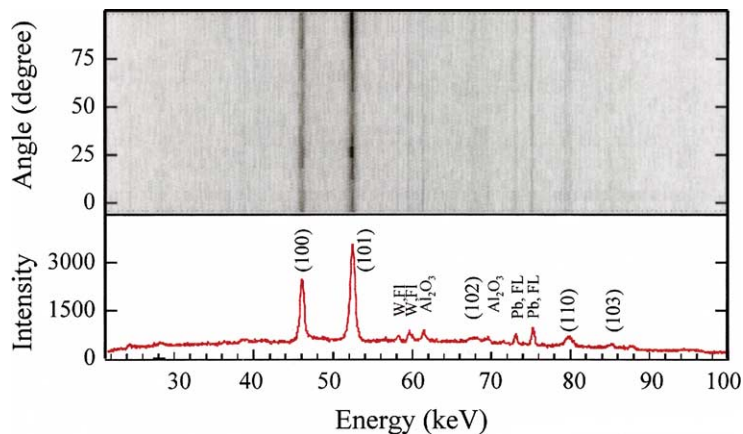


Fig. 7. X-ray diffraction image obtained with varying rotation angles and summed to give an integrated pattern.

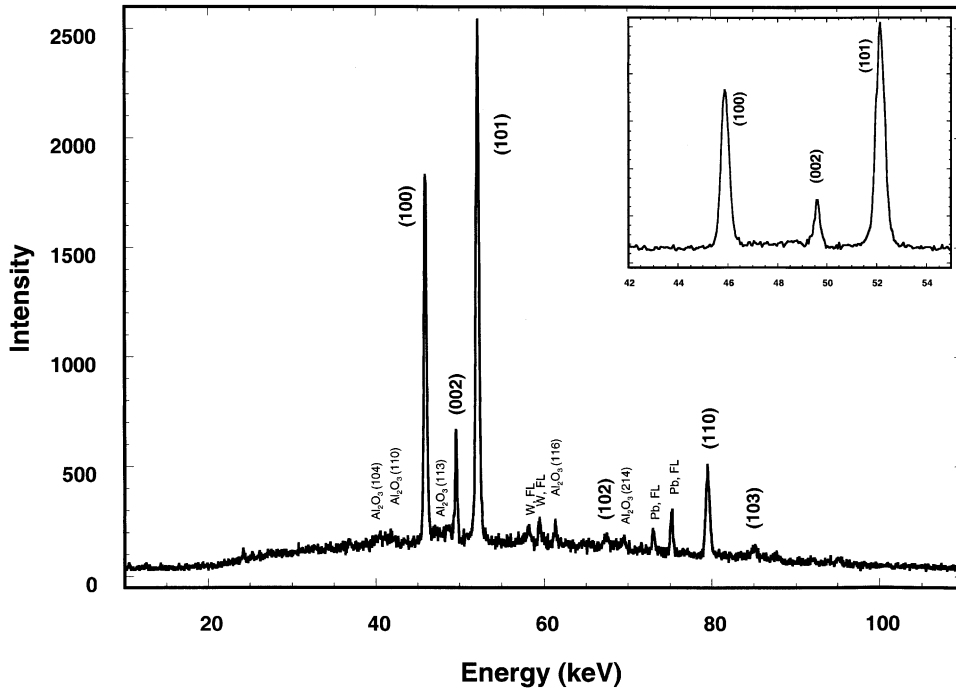


Fig. 8. X-ray diffraction pattern of iron at 161 GPa and 2450 K. Inset shows intense peaks of iron on a smaller scale. FL denotes fluorescence peaks.

$P$ – $T$  conditions in the sample and no coarse crystal formation. Fig. 8 is an integrated diffraction pattern of iron at 161 GPa and 2500 K. From this pattern, we can clearly observe five peaks from the h.c.p. phase, with refined parameters  $a = 2.238(1) \text{ \AA}$ ,  $c = 3.594(4) \text{ \AA}$ ,  $c/a = 1.605(7)$ , and  $V = 15.595(18) \text{ \AA}^3$ . At this  $P$ – $T$  point, the  $c/a$  ratio is very close to that at lower pressure (1.604) (Takahashi and Bassett, 1964). The intense peaks, (100) and (101), have linewidths (FWHM) of 378 and 384 eV, respectively, which are almost at the resolution limit of the detector (300 eV). This pattern demonstrates the existence of only the h.c.p. phase of iron under these  $P$ – $T$  conditions. Furthermore, from our experiments, we can only observe three solid phases in our  $P$ – $T$  range, b.c.c. at lower pressure, f.c.c. at higher temperature, and finally the h.c.p. phase. At pressures higher than 60 GPa (pressure at the  $\epsilon$ - $\gamma$ -liquid triple point), only two phases can be identified, the solid  $\epsilon$ -h.c.p. phase and the liquid. At this point there is no compelling experimental evidence for any other solid phase of iron stable between 1500 km depth and the inner core boundary (ICB).

We clearly observed a change in the relative intensities of the iron diffraction peaks in a limited temperature interval (marked in the phase diagram (Fig. 9)). At different times, the intensity of the most intense (100) and (101) peaks vary, and the (002) peak will appear and disappear. The peak positions also drift systematically under these conditions, indicating a small pressure change. No additional features (i.e., shoulders) or relative intensity changes can be observed when the patterns were collected after a sufficiently long time had elapsed for the system to reach equilibrium and the X-ray and laser beams were well aligned at the center of the sample. We believe that this phenomenon is caused by the relaxation of the sample inside the cell at high pressures and temperatures.

We selected different pressure media (Ar, NaCl,  $\text{Al}_2\text{O}_3$ , and MgO) to examine possible reactions between sample and medium. In runs with the above-described experimental configurations, we could clearly identify the expected phases of the pressure medium and the iron sample from the diffraction pattern. We did not observe other phases of iron.

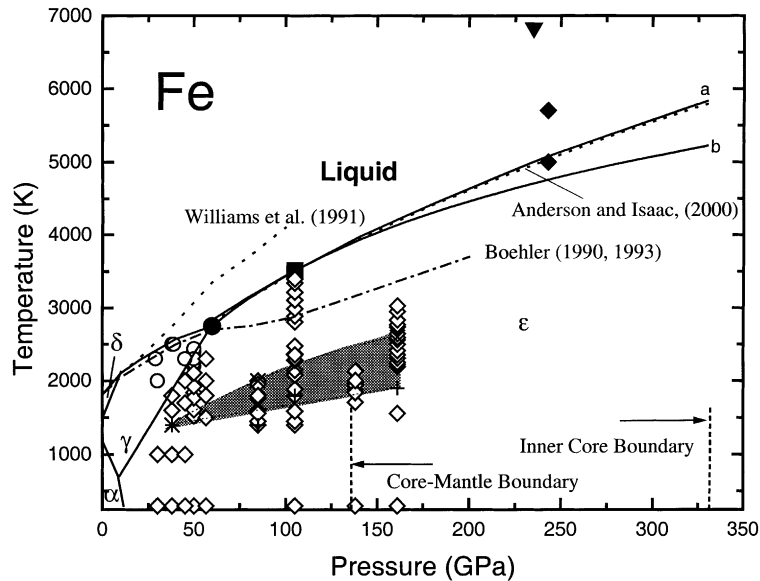


Fig. 9. Phase diagram of iron determined from this study. Open circles:  $\gamma$ -phase; open diamonds:  $\epsilon$ -phase; filled circle:  $\epsilon$ - $\gamma$ -liquid triple point; filled square: melting point; filled diamonds: melting points from shock compression data; filled triangle: melting point from Yoo et al. (1995). Curve (a): melting curves calculated using the Lindeman law; curve (b): melting curve calculated using the Kraut–Kennedy law. The shaded area shows the  $P$ - $T$  region where diffraction peaks change relative intensities (the cross marks the beginning temperature of these changes, and asterisk gives the ending point of such changes). Thermal pressure corrections are not accounted for this phase diagram. Williams et al., 1991; Anderson and Isaacs (2000); Boehler (1990, 1993).

Discounting the peaks due to the pressure media, the diffraction patterns collected with different media are entirely consistent with each other. Thus, we found no evidence for the pressure medium reacting with the iron sample at the high  $P$ - $T$  conditions studied.

### 3.3. $c/a$ ratio of $\epsilon$ -Fe

The  $c/a$  ratio of  $\epsilon$ -Fe has significant implications for the Earth's inner core. Recent first-principles calculations predict that the axial ratio of  $\epsilon$ -Fe increases substantially with temperatures, reaching 1.7 at a temperature of 5700 K (Steinle-Neumann et al., 2001). Fig. 10 shows the measured temperature dependence of  $c/a$  at 161 GPa, together with pressure dependence at 300 K up to that pressure. No systematic variation in  $c/a$  with temperature can be observed. The values for  $c/a$  fall between 1.596 and 1.608 Å (a range of 0.011), which is comparable to our experimental error. Though the calculations were carried out at higher pressures, the theoretical results suggest that temperature dependence is larger at lower pressures (i.e., ap-

proaching those of the present study). Furthermore, the pressure effect on  $c/a$  also is equally weak, consistent with previous experimental results, at pressures sufficiently above the  $\alpha$ - $\epsilon$  transition (Jephcoat et al., 1986; Mao et al., 1990). Additional high  $P$ - $T$  data are required to directly address the question of the  $c/a$  ratio and the associated elastic anisotropy of iron at inner core conditions. Nevertheless, the current comparison suggests the need for improved theoretical treatment of the elastic anisotropy of iron at high pressures and temperatures.

### 3.4. Melting line

When the temperature was raised to 3510 K at 105 GPa, we observed the loss of all diffraction peaks from iron, while the diffraction from the diamond remained persisted during continuous rotation of diamond anvil cell. This temperature reflects the lower bound on the melting point of iron (e.g., Shen et al., 1998), and is about 700 K higher than that obtained by Boehler (1993), and appears to be lower than the

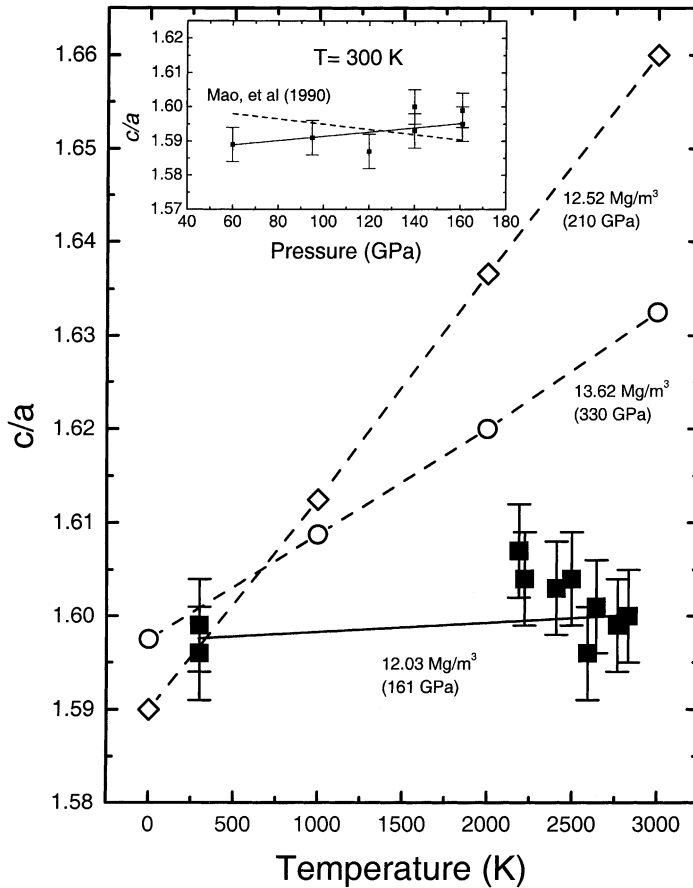


Fig. 10. Variation in the  $c/a$  ratio of  $\epsilon$ -Fe with temperature, at 161 GPa, (solid line) and comparison to theory (dashed lines; Steinle-Neumann et al., 2001). The inset shows the pressure dependence of  $c/a$  at 300 K (solid line) and earlier results (dashed line; Mao et al., 1990).

results of shock wave experiments. We now consider the application of various melting laws to the data. A simple linear extrapolation from the triple point at 60 GPa and 2750 K (Shen et al., 1998) to higher pressure yields a melting temperature above 7200 K at 328 GPa (ICB), which of course neglects the expected curvature in the melting line.

According to the Kraut–Kennedy law (Kraut and Kennedy, 1966),

$$T_m = T_{m0} \left( 1 + C \frac{\Delta V}{V_0} \right), \quad (1)$$

where  $T_m$  is the melting temperature at pressure  $P$ ,  $T_{m0}$  the melting temperature at ambient pressure,  $\Delta V/V_0$  the compression at pressure  $P$ , and  $C$  a constant. Using the equation of state determined by Mao et al. (1990)

to calculate the volume compression, along with our data above the  $\epsilon$ - $\gamma$ -liquid triple point, we determined the constant coefficients  $T_{m0}$  and  $C$  in Eq. (1) to be 551 K and 21.2, respectively. The extrapolated melting temperature of iron at 330 GPa is therefore 5220 K. Assuming that the uncertainty of our temperature measurement is  $\pm 100$  K, the error in melting temperature at the ICB is 320 K. In this calculation, thermal pressure and thermal expansion effects are not included.

Finally, consider the application of the Lindeman melting law, which has been more widely used. This melting relation is conventionally written as (Anderson and Isaak, 2000)

$$\frac{dT_m}{dP} = 2 \left( \frac{T_m}{K_T} \right) \left( \gamma - \frac{1}{3} \right).$$

The equation can be recast as

$$\frac{T_m}{T_{m0}} = \left(\frac{V}{V_0}\right)^{2/3} \exp\left\{\frac{2\gamma_0}{q} \left[1 - \left(\frac{V}{V_0}\right)^q\right]\right\},$$

where  $V/V_0$  corresponds to volume compression at high  $P$  and  $T$ , i.e., thermal pressure and thermal expansion have been taken into account. Our use of this formulation is close to that reported by Anderson and Isaak (2000), who used experimental data to fix  $T_m$  at low pressure (see Hemley and Mao, 2001a). Assuming  $q = 1$ , and using  $T_m = 3510$  K at 105 GPa, and  $\gamma_0 = 1.92$ , we obtain  $T_{m0} = 1608$  K. According to this formulation, the melting temperature of iron at ICB is 5830 K. Including uncertainties in the measured temperatures, the calculated temperature ranges from 5600 and 6000 K. This is an upper bound on the actual temperature of the ICB because of the melting point depression associated with the presence of other components; for further discussion and review, see Hemley and Mao (2001a).

### 3.5. Phase diagram

Fig. 9 shows the phase diagram of iron according to our experimental result and calculation of the melting line. As pointed out in Section 2.4, we observe only the  $\alpha$ -,  $\gamma$ -, and  $\epsilon$ -phases of iron within the high  $P$ - $T$  range studied. At lower pressures ( $<60$  GPa), our experimental results are consistent with those of Shen et al. (1998); thus no adjustment in the lower pressure phase boundaries, including the triple point, is required. The calculated melting curves from both the Kraut–Kennedy and Lindeman laws based on our experimental data are shown in the phase diagram with the curve calculated from thermochemical data by Anderson and Isaak (2000) for comparison. The  $\gamma$ - $\epsilon$ -liquid triple point from our calculation using the Lindeman law is 2835 K, which is also within the experimental error range when compared with the result of Shen et al. (1998). The calculated melting curve also falls within the range determined by Brown and McQueen (1986) based on shock wave experiments. This analysis also assumes that no new high  $P$ - $T$  phases exist; there is as yet no experimental evidence for such phases, though this has been the subject of some discussion in the literature (see Hemley and Mao, 2001a).

## 4. Conclusions

Resolution of the debates about the high  $P$ - $T$  phase relations of iron based on static pressure experiments requires careful analyses of experimental details in these challenging experiments. Our systematic tests indicate that there are many factors that can produce misleading experimental results, and care is required to evaluate their reliability. We believe that the most crucial factor is the existence of significant stress in samples arising from the high strength of iron at high pressures, which can produce considerable splitting of peaks in the measured diffraction patterns. Direct investigation of the iron phase diagram to 161 GPa and 3000 K reveals that the  $\epsilon$ -Fe is the only solid phase of iron at pressures beyond the  $\epsilon$ - $\gamma$ -liquid triple point. Direct measurements on the  $\alpha$ - and  $\gamma$ -phases were consistent with the previously determined triple point. Careful experimental study reveals no evidence of other solid phases at these conditions. At high temperatures but below the melting line, we observe a region where the diffraction peak intensities change. We ascribe this to the existence of a pressure-dependent temperature interval of stress release in the material. We extended the melting point measurement by X-ray diffraction to 105 GPa, and estimated the upper bound on the temperature at the inner core boundary to be between 5600 and 6000 K. Finally, measurements of the temperature dependence of the  $c/a$  ratio at high pressure indicate the need to examine theoretical predictions of the origin of the elastic anisotropy of the inner core.

## Acknowledgements

We would like to thank the staff of GSECARS at the Advanced Photon Source for their help with setting up the apparatus, and J. Hu and Q. Guo at beamline X17B of the National Synchrotron Light Source for useful discussions and experimental assistance. Thanks are also due to T.S. Duffy, G. Fiquet, and an anonymous reviewer for constructive comments. We are particularly grateful to S. Gramsch for careful reading of the manuscript. We thank NSF, NASA, DOE-BES, DOE-NNSA, and the W.M. Keck Foundation, for support.

## References

- Alfè, D., Gillan, M.J., Price, G.D., 1999. The melting curve of iron at the pressures of the Earth's core from ab initio calculations. *Nature* 401, 462–464.
- Alfè, D., Kresse, G., Gillan, M.J., 2000. Structure and dynamics of liquid iron under Earth's core conditions. *Phys. Rev. B* 61, 132–142.
- Anderson, O.L., 1990. The high pressure triple points and their effect on the heat flow from the Earth's core. *J. Geophys. Res.* 95, 21697–21707.
- Anderson, O.L., Isaak, D.G., 2000. Calculated melting curves for phases of iron. *Am. Miner.* 85, 376–385.
- Andraut, D., Fiquet, G., Kunz, M., Visocekas, F., Haeusermann, D., 1997. The orthorhombic structure of iron: an in situ study at high-temperature and high-pressure. *Science* 278, 831–834.
- Boehler, R., 1986. The phase diagram of iron to 430 kbar. *Geophys. Res. Lett.* 13, 1153–1156.
- Boehler, R., 1993. Temperature in the Earth's core from melting point measurement of iron at high static pressure. *Nature* 363, 534–536.
- Boehler, R., 2000. High-pressure experiments and the phase diagram of lower mantle and core materials. *Rev. Geophys.* 38, 221–245.
- Brown, J.M., McQueen, R.G., 1986. Phase transitions, Grüneisen parameter, and elasticity for shocked iron between 77 and 400 GPa. *J. Geophys. Res.* 91, 7485.
- Dubrovinsky, L., Saxena, S.K., Lazor, P., Weber, H.-P., 1998. Structure of  $\beta$ -iron at high temperature and pressure. *Science* 281, 11a.
- Dubrovinsky, L.S., Saxena, S.K., Tutti, F., Rekki, S., Le Bihan, T., 2000. In situ X-ray study of thermal expansion and phase transition of iron at multimegabar pressure. *Phys. Rev. Lett.* 84, 1720–1723.
- Hemley, R.J., Mao, H.K., 2001a. In situ studies of iron under pressure: new windows on the Earth's core. *Int. Geol. Rev.* 43, 1–26.
- Hemley, R.J., Mao, H.K., 2001b. Progress in cryocrystals to megabar pressures. *J. Low Temp. Phys.* 122, 331–344.
- Hemley, R.J., Chiarotti, G., Bernasconi, M., Ulivi, L. (Eds.), 2002. *Proceedings of the International School of Physics "Enrico Fermi" on High-Pressure Phenomena, Course CXLVII.* IOS Press, Amsterdam.
- Jephcoat, A.P., Mao, H.K., Bell, P.M., 1986. The static compression of iron to 78 GPa with rare gas solids as pressure-transmitting media. *J. Geophys. Res.* 91, 4677–4684.
- Kavner, A., Duffy, T.S., 2001. Pressure–volume–temperature paths in the laser-heated diamond anvil cell. *J. Appl. Phys.* 89, 1907–1914.
- Kraut, E.A., Kennedy, G.E., 1966. Melting law for high pressure. *Phys. Rev.* 151, 668–675.
- Ma, Y., Somayazulu, M., Mao, H.K., Hemley, R.J., Gramsch, S.A., Shen, G., Somayazulu, M., 2001. Two-dimensional energy dispersive X-ray diffraction at high pressures and temperatures. *Rev. Sci. Instrum.* 72, 1302–1305.
- Mao, H.K., Bell, P.M., Hadidiacos, C., 1987. Experimental phase relations of iron to 360 kbar and 1400 °C, determined in an internally heated diamond anvil apparatus. In: Manghnani, M.H., Syono, Y. (Eds.), *High Pressure Research in Mineral Physics.* Terra Scientific/AGU, Washington, DC, pp. 135–138.
- Mao, H.K., Wu, Y., Chen, L.C., Shu, J.F., Jephcoat, J.P., 1990. Static compression of iron to 300 GPa and Fe<sub>0.8</sub>Ni<sub>0.2</sub> alloy to 260 GPa: implications for composition of the core. *J. Geophys. Res.* 95, 21737.
- Mao, H.K., Shen, G., Hemley, R.J., Duffy, T.S., 1997. X-ray diffraction with a double hot plate laser-heated diamond cell. In: Manghnani, M.H., Syono, Y. (Eds.), *High-Pressure Research in Mineral Physics: Application to Earth and Planetary Sciences.* Terra Scientific/AGU, Washington, DC, pp. 27–34.
- Mao, H.K., Shu, J., Shen, G., Hemley, R.J., Li, B., Singh, A.K., 1998. Elasticity and rheology of iron above 220 GPa and the nature of the Earth's inner core. *Nature* 396, 741–743.
- Meade, C., Jeanloz, R., 1988. Yield strength of the B1 and B2 phases of NaCl. *J. Geophys. Res.* 93, 3270–3274.
- Saxena, S.K., Dubrovinsky, L.S., Haggkvist, P., Cerenius, Y., Shen, G., Mao, H.K., 1995. Synchrotron X-ray study of iron at high pressure and temperature. *Science* 269, 1703–1704.
- Shen, G., Heinz, D.L., 1998. High-pressure melting of deep mantle and core materials. In: Hemley, R.J. (Ed.), *Ultra-high-Pressure Mineralogy, Reviews in Mineralogy.* Mineralogical Society of America, Washington, DC, pp. 369–396.
- Shen, G., Mao, H.K., Hemley, R.J., Duffy, T.S., Rivers, M.L., 1998. Melting and crystal structure of iron at high pressures and temperatures. *Geophys. Res. Lett.* 25, 373–376.
- Shen, G., Rivers, M., Wang, Y., Sutton, S., 2001. Laser heated diamond cell system at the Advanced Photon Source for in situ X-ray measurements at high pressure and temperature. *Rev. Sci. Instrum.* 72, 1273–1282.
- Shim, S.H., Duffy, T.S., Shen, G., 2000. The equation of state of CaSiO<sub>3</sub> perovskite to 108 GPa at 300 K. *Phys. Earth Planet. Interiors* 120, 327–338.
- Song, X.D., Helmlinger, D.V., 1993. Anisotropy of Earth's inner core. *Geophys. Res. Lett.* 20, 2591–2594.
- Steinle-Neumann G., Stixrude, G.L., Cohen, R.E., Gülseren, O., 2001. Elasticity of iron at the temperature of the Earth's inner core. *Nature* 413, 57–60.
- Sung, C.M., Goetze, C., Mao, H.K., 1977. Pressure distribution in the diamond anvil press and the shear strength of fayalite. *Rev. Sci. Instrum.* 48, 1386–1391.
- Takahashi, T., Bassett, W.A., 1964. High pressure polymorph of iron. *Science* 145, 483–486.
- Williams, Q., Jeanloz, R., Bass, J., Svendsen, B., Ahrens, T.J., 1987. The melting curve of iron to 250 GPa: a constraint on temperature at Earth's center. *Science* 236, 181–183.
- Yoo, C.S., Holmes, N.C., Ross, M., 1993. Shock temperatures and melting of iron at Earth core conditions. *Phys. Rev. Lett.* 70, 3931–3934.
- Yoo, C.S., Akella, J., Campbell, A.J., Mao, H.K., Hemley, R.J., 1995. Phase diagram of iron by in situ X-ray diffraction: implication for the Earth's core. *Science* 270, 1473–1475.
- Yoo, C.S., Akella, J., Campbell, A.J., Mao, H.K., Hemley, R.J., 1997. Detecting phases of iron. *Science* 275, 94–96.